Title: The character and amplitude of 'discontinuous' bottom-simulating reflections in marine seismic data

Journal: Earth and Planetary Science Letters

Authors: Hillman, Jess I T [a], Cook, Ann E [a], Sawyer, Derek E [a], Küçük, H. Mert [b,c] and Goldberg, David, S [c].

Affiliations: [a] School of Earth Sciences, The Ohio State University, 125 South Oval Mall, Columbus OH 43210, USA. (jithillman@gmail.com), [b] Dokuz Eylül University, Institute of Marine Sciences and Technology, Haydar Aliyev Blv., 35340 Inciralti, Izmir, Turkey, [c] Lamont-Doherty Earth Observatory, 61 Route 9W, Palisades, NY 10964, USA.

Abstract:

Bottom-simulating reflections (BSRs) identified in seismic data are well documented; and are commonly interpreted to indicate the presence of gas hydrates along continental margins, as well as to estimate regional volumes of gas hydrate. A BSR is defined as a reflection that sub-parallels the seafloor but is opposite in polarity and cross-cuts dipping sedimentary strata. BSRs form as a result of a strong negative acoustic impedance contrast. BSRs, however, are a diverse seismic phenomena that manifest in strikingly contrasting ways in different geological settings, and in different seismic data types.

We investigate the characteristics of BSRs, using conventional and high resolution, 2D and 3D seismic data sets in three locations: the Terrebonne and Orca Basins in the Gulf of Mexico, and Blake Ridge on the US Atlantic Margin. The acquisition geometry and frequency content of the seismic data significantly impact the resultant character of BSRs, as observed with depth and amplitude maps of the BSRs. Furthermore, our amplitude maps reinforce the concept that the BSR represents a zone, over which the transition from hydrate to free gas occurs, as opposed to the conventional model of the BSR occurring at a single interface.

Our results show that a BSR can be mapped in three dimensions but it is not spatially continuous, at least not at the basin scale. Rather, a BSR manifests itself as a discontinuous, or patchy, reflection and only at local scales is it continuous. We suggest the discontinuous nature of BSRs is the result of variable saturation and distribution of free gas and hydrate, acquisition geometry and frequency content of the recorded seismic data. The commonly accepted definition of a BSR should be broadened with careful consideration of these factors, to represent the uppermost extent of enhanced amplitude at the shallowest occurrence of free gas trapped by overlying hydrate-bearing sediments.

1.0 Introduction:

Bottom-simulating reflections (BSRs) identified in seismic data are well documented, and have been used to indicate the presence of gas hydrates in continental slope environments since they were first identified at the Blake Ridge in the 1970s (Bryan, 1974; Shipley et al., 1979). BSRs are defined in seismic data as reflections that sub-parallel the seafloor, cross cut dipping sedimentary strata, and in the case of hydrate related BSRs, are opposite in polarity to the seafloor (Guerin et al., 1999; Holbrook et al., 1996; Shipley et al., 1979). The majority of documented BSRs are interpreted to be the result of a negative impedance caused by the transition from gas hydrate bearing sediments above the base of gas hydrate stability (BGHS), to free gas bearing sediments below (Haacke et al., 2007; Max and Dillon, 1998; Petersen et al., 2007; Shedd et al., 2012). The shallowest occurrence of gas is dependent on the local supersaturation of methane within a local gas stability zone (Xu and Ruppel, 1999). In the literature the term bottom-simulating reflector is sometimes used, rather than bottom-simulating reflection. A reflector is a physical boundary at which a reflection occurs; whereas the BGHS or top of free gas is a physical horizon off which seismic energy reflects, forming a BSR, therefore the term bottom-simulating reflection is more accurate. In a seismic profile we observe reflections, which can be described in terms of attributes such as amplitude. Such properties cannot be assigned to a reflector.

Previous studies have proposed several primary geological controls on the presence of free gas below the BGHS, and therefore the observation of a BSR. These are, the pressure and temperature conditions, the

rate of tectonic uplift of the seafloor, lithology and the rate of upward fluid flux (Chapman et al., 2002; Haacke et al., 2007; Shedd et al., 2012; Wood and Gettrust, 2000).

The location of the BGHS is dependent primarily on pressure and temperature conditions, which are unlikely to vary dramatically across localized scales (Clennell et al., 2000; Wood et al., 2008). Porewater salinity and gas composition are also controlling factors, and these may vary locally, resulting in the formation of pluming BSRs, such as are observed in the Gulf of Mexico (Clennell et al., 1999; Liu and Flemings, 2007; Shedd et al., 2012). Other factors including grain surface effects and pore size may have a more limited impact on the position of the BGHS (Daigle and Dugan, 2014). The interaction of these factors determines the thermodynamic state, growth kinetics, spatial distribution and growth state of gas hydrate (Clennell et al., 1999). Although the definition implies that a BSR must be 'bottom simulating', a BSR will only mirror the seafloor in areas where the temperature conditions (isotherms) are dominated by conduction, not advection.

Nevertheless, BSRs are commonly used to interpret the presence of gas hydrate and / or free gas in many different settings (Bünz et al., 2003; Hornbach et al., 2008; McConnell and Kendall, 2013), although the exact nature of these parameters are often not clearly understood, and gas hydrate occurrences have been documented in the absence of BSRs (Haacke et al., 2007; Majumdar et al., 2016; Paganoni et al., 2016). Such complicating factors have motivated this review of the physical nature of the characteristics of BSRs. As described by Shedd et al. (2012) there are three types of BSR that are attributed to the presence of gas hydrates and can be characterized in seismic reflection data; continuous (Fig. 1a and b), discontinuous (Fig. 1c and d), and pluming BSRs. Continuous BSRs are the classic feature, characterized by a continuous, coherent event that cross-cuts primary stratigraphy, a typical, well known example would be the Blake Ridge (Shipley et al., 1979). In some regions continuous BSRs are relatively rare, in the Gulf of Mexico, for example, the most common is discontinuous. Unlike the continuous BSR, a discontinuous or segmented BSR is characterized by spaced anomalous seismic events that are generally parallel to seafloor bathymetry (McConnell and Kendall, 2013; Shedd et al., 2012). Pluming BSRs are

characterized as a continuous reflection that does not follow seafloor geomorphology, but are bowed towards the seafloor as a result of significant, locally constrained increases in heat flow related to strong vertical fluid flux (Shedd et al., 2012). Pluming BSRs occur as small scale, localized anomalies; as such, these features will not be discussed further in this study.

A fourth type of BSR, known as diagenetic BSRs, form as the result of diagenetic boundaries in siliceous sediments where sediment density increases with depth, most commonly due to the transformation of biogenic silica (opal-A) to opal-CT (Berndt et al., 2004; Davies and Cartwright, 2002; Goldberg et al., 1987). The acoustic impedance associated with the relative change in density results in a prominent reflection with the same polarity as the seafloor; this reflection follows an isothermal gradient, and therefore parallels seafloor topography (Davies and Cartwright, 2002; Lee et al., 2003). This is unlike BSRs caused by free gas and/or gas hydrate, where the reflection is the opposite polarity of the seafloor reflection.

Herein, we characterize BSRs associated with the presence of gas hydrate in three locations to understand the impact of hydrate and free gas saturation, geological characteristics, and acquisition parameters of the seismic data on the appearance of BSRs in marine seismic data. The Blake Ridge on the US Atlantic margin, although by no means the largest hydrate occurrence worldwide, is perhaps the most well-known, (e.g. Gorman et al., 2002; Hornbach et al., 2008, 2003; Markl et al., 1970). We selected this site as it is the textbook example of a continuous BSR, and multiple seismic datasets have been acquired in the area. Our other two locations, the Terrebonne mini-basin and the Orca Basin, provide classic examples of discontinuous BSRs in the northern Gulf of Mexico. The Terrebonne mini-basin has been the site of several previous gas hydrate studies (Boswell et al., 2012b; Frye et al., 2012), most notably the Joint Industry Project (JIP) II in 2009, when two wells were drilled and logging-while-drilling (LWD) data were acquired. Both the Terrebonne mini-basin and the Orca Basin are being evaluated as proposed drill sites in the Gulf of Mexico Generation of Methane [GOM]^2 project, currently under review by the

International Ocean Discovery Program (IODP), and multiple seismic data sets have also been acquired at each of these sites.

In each of these locations we use 3D seismic data to map out and characterize the BSR, producing depth and amplitude maps. In addition, at the Terrebonne site, we use high-resolution 2D seismic data to investigate the differences associated with data acquisition geometry and frequency content on the characteristics of the mapped BSR. Mapping BSRs in 3D seismic data allows us to determine the potential areal extent of gas hydrate occurrence, which, in combination with well data, is a valuable tool in constraining volumetrically the quantity of methane hydrate in a region (Hornbach et al., 2008). Mapping BSRs using 2D seismic data with a higher frequency content, provides enhanced stratigraphic detail near the base of hydrate stability, indicated by BSRs that have a distinct character, which also provides a critical tool for defining the location and disposition of hydrate in sedimentary layers (Haines et al., 2014). One of the primary factors that determine how a feature is imaged in seismic data is the frequency content of the data, and the corresponding resolution. The resolution of seismic data refers to the minimum separation of two features at which they can be resolved as multiple interfaces (Bulat, 2005; Hyndman and Spence, 1992; Wood et al., 2008). The lateral resolution of the data, commonly referred to as the Fresnel zone, is defined for vertically travelling waves as the area within which the reflected waves interfere constructively, resulting in energy being averaged and coherently reflected back towards the receiver (Wood et al., 2008; Yilmaz, 2001). The size of the Fresnel zone is dependent on the wavelength of the seismic signal and the depth to the reflector. In this study, we refer to conventional 3D data, with a typical frequency content in the 10-80 Hz range and high-resolution data in the 80-250 Hz range (Chapman et al., 2002; Petersen et al., 2007; Wood et al., 2002; Wood and Gettrust, 2000).

We present maps of BSRs derived from 3D seismic data, including previously unpublished amplitude maps. The results highlight the significant influence that seismic acquisition geometry and frequency content have on the resultant BSR characteristics, and call into question the widely accepted definition of a BSR. The BSRs in our study areas do not fit the definition as they do not consistently follow seafloor

bathymetry, and depending on the resolution of the seismic data, they are not characterized as discrete reflections.

1.1 Geological setting

The seabed morphology of the northeast Gulf of Mexico is characterized by salt-bounded mini-basins, typically infilled by Miocene-Pleistocene strata (Diegel et al., 1995; Frye et al., 2012; Pilcher and Blumstein, 2007). The geomorphology of these mini-basins is due to the coeval processes of relative salt rise on the flanks, and subsidence at the center (Diegel et al., 1995; Worrall and Snelson, 1989). The Terrebonne and Orca Basins are salt bounded mini-basins in the Walker Ridge (WR) protraction area in the Gulf of Mexico, lying in water depths of 1500-2000m (Boswell et al., 2012b; Frye et al., 2012) (Fig. 2). Both the Terrebonne and Orca Basins have been infilled by a sedimentary sequence consisting of increasingly mud rich units with occasional interbedded thin sands of Miocene to Pliocene age(Boswell et al., 2012b; Frye et al., 2012; Haines et al., 2014).

The Blake Ridge is a large contourite drift deposit, located ~450 km off the coast of the Carolinas in water depths of 2000-4000 m (Fig. 2) (Holbrook et al., 2002; Hornbach et al., 2008, 2003; Wood and Gettrust, 2000). This region has been extensively studied with regards to gas hydrate, due to presence of a clear, prominent BSR. In addition, the geology of the Blake Ridge is relatively homogeneous; the ridge consists of near uniform fine silts and mudstones, and correlation of well data to seismic data has shown limited lateral variation in lithology across the area (Clennell et al., 2000; Hornbach et al., 2008).

2.0 Methods

2.1 Seismic data acquisition

We use data acquired by five different surveys (see Appendix A for details of seismic acquisition), two of these surveys, at Terrebonne and Orca, are industry acquired conventional 3D seismic surveys. In addition, we use 2D data and pseudo-3D acquired by research cruises at Terrebonne, Orca Basin and Blake Ridge.

147 *2.2 Seismic data processing*

148 The onboard processing sequence for both conventional 3D data sets used in this study included:
149 geometry definition and correction, trace editing, receiver motion compensation, navigation merge,
150 application of a 6.25 x 60 m grid and noise attenuation (Janos and Zhang, 2012; Waughman and
151 O'Connor, 2007). Further processing included: 3D generalized surface multiple prediction (GSMP) and
152 least squares adaptive subtraction, residual multiple attenuation, seismic interference noise elimination,
153 residual anomalous amplitude attenuation, water velocity correction, residual wavelet shaping and
154 migration data preparation. The processed conventional 3D data were also subsampled prior to
155 interpretation. For the Orca Basin data, a high-resolution Kirchoff sediment flood migration was then
156 conducted, followed by multi-azimuth sediment tomography, subsalt tomographic velocity updates and
157 depth migration (Janos and Zhang, 2012). For the Terrebonne data, a wavefield extrapolation migration
158 was conducted. We converted the depth volume at Terrebonne back to a time volume using a 3D velocity
159 model in IHS Kingdom®.

160 The high-resolution pseudo-3D volume at Blake Ridge was created using bin sizes of 37.5 m (inline) and
161 75 m (crossline). Stacking velocities were determined using semblance analysis, these velocity picks were
162 then used to create a 3D velocity model (Hornbach et al., 2008). An initial pre-stack depth migration of
163 the volume was generated, followed by band pass filtering and normalization of traces (Hornbach et al.,
164 2008).

165 Conventional seismic data processing techniques were applied to 2D high-resolution seismic
166 data acquired at Terrebonne. Processing steps for the 2D data included: raw data loading,
167 geometry definition using shot-receiver geometry and real shot coordinates, trace editing/muting,
168 f-k dip filtering, inline sorting, velocity analysis and 2D prestack Kirchoff time migration (See
169 Appendix B for details of processing).

170 *2.2.1 Mapping in 3D*

171 At each of the three locations, the available 3D processed seismic data were used to map the BSR on a
172 line-by-line basis. Examination of the data at Terrebonne and Orca Basin showed that the BSR was most
173 readily identified on crosslines and inlines respectively; these were therefore primarily used for mapping
174 of the BSR. Only inlines and crosslines are used for mapping due to the presence of minor vertical
175 artifacts in arbitrary lines. At Blake Ridge, the quality of the crossline data is very poor due to the pseudo-
176 3D nature of the data; therefore only inlines were used for mapping the BSR. Mapped horizons were then
177 used to generate maps of each horizon.

178 **3.0 Results**

179 At each location we present structural depth and amplitude maps of the seafloor and the BSR, mapped
180 from the 3D seismic data, in addition to seismic profiles showing the typical appearance of the BSR. The
181 bathymetry of the Blake Ridge region is characterized by large sediment drift deposits to the west of the
182 area, gradually sloping to the east where the geomorphology is relatively flat (Fig. 3). The strata tend to
183 dip at a low angle of ~2-6° where they intersect the BSR. In these high-resolution data, the BSR at Blake
184 Ridge is characterized as a 'continuous' BSR across the majority of the area; however, it deteriorates into
185 a more discontinuous BSR to the east (Fig. 3) as previously identified by Hornbach et al., (2008). This
186 change in the nature of the BSR correlates to a change in the geomorphology of the basin, moving away
187 from the sediment wave field in the east.

188 The seafloor geomorphology of the Terrebonne and Orca Basins is typical of salt bounded mini basins in
189 the Gulf of Mexico. Bathymetric highs mark the position of salt-cored ridges that bound the basins, while
190 the sediments of the infilled basins are gently dipping. The BSR at Terrebonne and Orca Basin is a
191 discontinuous BSR, clearly visible in the conventional 3D seismic data as a reflection that parallels the
192 seafloor geomorphology. At Terrebonne, the BSR is associated with an amplitude change and phase
193 reversal of dipping sedimentary units as they cross the BSR (Fig. 4a and 5). Unlike Terrebonne, however,
194 the BSR at Orca is not always associated with a phase reversal in the dipping sediment reflections (Fig.
195 4d and 6).

196 At Terrebonne, the BSR is readily identifiable in crosslines of the conventional 3D volume, that are
197 oriented NW-SE and cross-cut the dipping sedimentary units along strike (Fig. 4a). However, in the
198 orthogonal inlines, the BSR is difficult to identify as these lines are oriented NE-SW along the strike of
199 the sedimentary units. The BSR therefore does not cross-cut the sediments clearly as they are sub-
200 horizontal in this orientation. The sediments in the Terrebonne Basin dip at an angle of ~11-19° where
201 they intersect the BSR. At Orca, as at Terrebonne, the BSR is more readily identified in one orientation
202 than the other: it is clearly visible in seismic inlines oriented NE-SW as these lines cross cut the
203 sediments perpendicular to strike (Fig. 4d and 6a). The strata in the Orca Basin dip at an angle of ~12-26°
204 where they intersect the BSR.

205 The structure of the BSR at both Gulf of Mexico locations closely follows that of the seafloor, with an
206 average depth of ~900 mbsf at Terrebonne, and ~590 mbsf at Orca (Fig. 4). The amplitude of the BSR is
207 most prominent in bands around the basins (Fig. 4a and 4b). At Terrebonne, these bands correlate to
208 where the BSR crosses known coarse grained units (Frye et al., 2012) producing a distinct BSR where it
209 can be mapped as a reflection (Fig. 4a and b). Although we do not have amplitude data at Blake Ridge
210 (Fig. 3), it is possible to see the contrast between this location and the Gulf of Mexico sites, with a much
211 patchier distribution of the mapped BSR at Terrebonne and Orca (Fig. 4b and 4c). The greatest distance
212 across which the BSR can be imaged as a continuous feature at each location is 1) 26.54 km Blake Ridge,
213 2) 6.97 km Terrebonne and 3) 11.51 km at Orca Basin.

214 The Blake Ridge seismic data is a pseudo-3D volume (Hornbach et al., 2008), and we find that the
215 amplitude values in the seismic data are inconsistent across lines. Therefore we are unable to produce
216 amplitude maps of the BSR and seafloor at this location. The geomorphology of the BSR closely
217 resembles that of the seafloor at Blake Ridge, dipping gradually to the east, with an average depth of ~520
218 mbsf. In the southwestern area of the data set, the BSR reflects the undulating topography of the seafloor
219 (Fig. 3).

At Terrebonne there is a strong contrast in the nature of the BSR in conventional 3D seismic data relative to high-resolution 2D seismic data (Fig. 5). In 2D data, the BSR can be identified by the same characteristics as in the 3D data: phase reversal of the dipping sediments and increased amplitude of these units below the BSR (Fig. 5e and f); however, the finer vertical and lateral resolution of the 2D data results in more discontinuous reflections along a seismic line. Even though discontinuous BSRs appear as aligned terminations of stronger amplitudes on conventional 3D seismic profiles along the base of the hydrate stability zone (BGHSZ) (Fig. 4a and 4d), the high-resolution 2D data show finer details of the strata where discontinuous BSRs are observed. Used in conjunction with the conventional 3D seismic data, high-resolution 2D data provide additional information on the BSR morphology and a better understanding of the finer structure of the hydrate stability field within the sedimentary column. Unlike Terrebonne, the BSR is readily identified in the 2D data at this site (Fig. 6c); however, the 2D data at this location have a much lower frequency content in comparison to the high-resolution 2D data at Terrebonne.

4.0 Discussion

The current definition of a BSR implies a continuous reflection, but the examples presented here demonstrate that, when observed in a wider spatial context, these features are in fact discontinuous at basin scales. Further, even at Blake Ridge, possibly the most well-known example of a continuous BSR, the BSR at this location is clearly fragmented across the extent of the data set (Fig. 3b), and when observed in ultra-high resolution data, becomes inconsistent and patchy (Wood et al., 2002; Wood and Gettrust, 2000). Likewise, the discontinuous BSR at Terrebonne becomes even more discrete when observed in high frequency 2D data (Fig. 5). We therefore argue that all BSRs are more accurately described as discontinuous in nature due to the complex interaction of the factors controlling them. Features defined as continuous BSRs are only imaged as such across limited spatial extents due to the comparatively low resolution of the data in which they are observed.

It is commonly assumed that the position of a BSR coincides with the base of gas hydrate stability (BGHS), and that a BSR can be interpreted as the depth at which hydrate is no longer stable due to increased pressure and temperature (Bünz et al., 2003; Paganoni et al., 2016). At this interface, free gas accumulates beneath the hydrate layer, creating a strong acoustic impedance that is imaged in seismic data as a BSR (Haacke et al., 2007; Holbrook et al., 1996; Max and Dillon, 1998). In reality, it is more accurate to say that, rather than a step-change from hydrate above, to free gas below, the BSR marks the first occurrence of free gas and is not a discrete plane, but a phase boundary interval of finite thickness, or transition zone (Clennell et al., 1999; Guerin et al., 1999).

In addition, the assumed requirement that free gas exists at BGHS has been shown to not be necessary, and gas hydrate may not be present near the base of gas hydrate stability (Daigle and Dugan, 2014; Xu and Ruppel, 1999). Free gas may occur near the BGHS, or even deeper, depending on the relationship between fluid flux and the local solubility threshold. In this case, the BSR may not coincide with the thermodynamic base of hydrate stability, but still represents the shallowest free gas (Guerin et al., 1999). As discussed by Xu and Ruppel (1999), hydrate can only accumulate where the mass fraction of methane remains in excess of local methane solubility, therefore the relative positioning of the BSR (shallowest free gas), actual hydrate occurrence and the BGHS is dependent on; 1) the methane flux rate, 2) the solubility of methane and localized conditions of grain scale saturation, 3) porosity and 4) permeability. Below the BSR, in the transition zone, there may be either hydrate and free gas co-existing in patchy distribution (Guerin et al., 1999; Liu and Flemings, 2007), or water saturated sediments in which neither free gas or hydrate are present (Xu and Ruppel, 1999). Previous publications have proposed that under the right conditions, a BSR could form in the absence of free gas, possibly as a result of gas hydrate bearing sediments overlying water saturated sediments (Holbrook et al., 1996; Hyndman and Spence, 1992).

If the transition zone is thin, such as an abrupt change from gas hydrate to free gas, it may be imaged as a discrete BSR in most datasets. However, if this zone is more extensive and diffuse, then the BSR may be imaged as a distinct horizon in lower resolution data, but in high-resolution data it may be resolved into a

series of lower amplitude units (Boswell et al., 2012b; Chapman et al., 2002; Guerin et al., 1999; Lee et al., 1994; Petersen et al., 2007; Shedd et al., 2012; Wood et al., 2002). The vertical scale of this transition zone is predominantly controlled by regional pressure and temperature conditions, and such factors are unlikely to vary over localized scales. Other factors such as hydrate distribution and lithology may vary across small scales, particularly where sediments are dipping. There may be irregularities in the lateral stability boundary as a result of perturbations in fluid and heat flux, pore size, lithology etc. (Liu and Flemings, 2007). This is clearly illustrated in the amplitude maps of the BSR at Terrebonne and Orca Basins (Fig. 4b and 4c), which show distinct lateral variability in the appearance and amplitude of the BSR.

The nature of the BSR is dependent on the complex interaction of numerous factors. The key factors that we address here are gas hydrate and free gas saturation, formation characteristics such as lithology and permeability, seismic acquisition geometry and corresponding survey resolution, and the orientation of the survey lines relative to the geomorphology of the strata in which hydrate occurs. These factors are intrinsically linked, as the formation characteristics are a primary factor in controlling the volume and rate of hydrate formation, the supply of methane to the formation, and the volume of gas accumulating below the BSR (Guerin et al., 1999). Further, factors related to seismic survey design may have a large impact on the characterization of the BSR. The variation in the seismic acquisition geometry and acquisition frequency of surveys discussed in this study is summarized in Fig. 7. All of these aspects of the seismic acquisition must be taken into account when designing a survey, and subsequently interpreting the acquired data.

4.1 Formation characteristics

The sediments at Blake Ridge in which hydrates have been identified are relatively homogeneous contourite drift deposits, primarily composed of near-uniform fine grained silt and mudstones (Holbrook et al., 1996; Hornbach et al., 2008; Paull et al., 1996), whereas, the two sites in the Gulf of Mexico are characterized by distinctly heterogeneous sedimentary sequences. At Blake Ridge, the relative

294 homogeneity of the lithology (and associated hydrate occurrence) is likely contributing to the extensive,
295 uninterrupted sections of BSR observed in our dataset (Fig. 3). In contrast, the sedimentary sequence
296 infilling the Terrebonne Basin consists of interbedded muds and sands, with increasingly mud rich units
297 moving up through the sequence (Frye et al., 2012). The deeper sand units are interpreted as channel-
298 levee systems with ponded sands deposited in a closed basin setting (Boswell et al., 2012b; Frye et al.,
299 2012). Similarly, the sediments infilling Orca Basin are interpreted as interbedded sand and mud rich
300 units of variable thicknesses, based on correlation to industry well data. Several sand units were identified
301 in well data from the west of the survey area in WR143-001 and WR143-003. It is in these thicker sand
302 units in both Gulf of Mexico locations that the BSR is most clearly imaged in the conventional 3D
303 seismic data. The BSR appears as a strong reflection where it cross-cuts high amplitude reflections that
304 correlate to proven sand rich units from well data at Terrebonne. A similar pattern is seen in the high-
305 resolution 2D data at Terrebonne (Fig. 4), although the BSR is less convincing than observed in the
306 conventional 3D data, it is clearest where it crosses the sand units. This suggests that the lithology at these
307 sites has a significant influence on the formation and imaging of the BSR.

308 *4.2 Gas hydrate and free gas occurrence*

309 The results of drilling and sampling Blake Ridge and LWD at Terrebonne revealed that the gas hydrate
310 system is dramatically different at both locations. As only a few industry well logs were available in our
311 Orca dataset, we focus on Terrebonne and Blake Ridge in this discussion. At Blake Ridge, previous
312 studies by Guerin et al. (1999) and Ecker et al. (2000) estimate the saturation of free gas below the GHSZ
313 to be 1-5% of pore volume below the BSR. This is consistent with studies elsewhere that have shown that
314 minimal concentrations of free gas may be sufficient to cause a drop in compressional velocity, and
315 therefore result in the formation of a BSR (Andreassen et al., 1995; Murphy et al., 1993; Wood et al.,
316 2008). Guerin et al. (1999) provide an estimate of 5-10% hydrate saturation, based on LWD data from
317 ODP Site 995. This value is corroborated by a piston core sample from the same location with a hydrate
318 saturation of 8%, and is consistent with estimates from other studies (e.g. Holbrook et al., 1996).

In contrast to Blake Ridge, LWD data at Terrebonne revealed substantially higher saturations of gas hydrate, albeit focused in specific units. Using LWD data from the JIP II wells at Terrebonne it is possible to estimate the gas hydrate saturation in the GHSZ. Frye et al. (2012) estimate that 4.4 x 10^9 m^3 of gas in hydrates is present in the GHSZ within thick sand bodies, with hydrate saturations of 75-90% (Boswell et al., 2012a). Lower saturations of hydrate are present in thinner sand units (~60%), and in the mud rich fractured unit in the upper stratigraphy (2-8%) (Cook et al., 2014). The average gas concentration in hydrates across the basin is estimated to be 1.183 x 10^9 m^3 km^2 where sands are present, and 0.32 10^9 m^3 km^2 where sands are absent (Frye et al., 2012). The JIP II wells did not drill into the gas leg underlying the BSR due to the risks associated with drilling free gas using a riserless drill ship; however, we would expect there to be a similar saturation of free gas below the BSR as there is of gas in hydrate above the BSR. The results of the JIP II expedition revealed significant volumes of gas present in hydrate within the GHSZ at Terrebonne; therefore it is likely that the saturation of hydrate and free gas is a controlling factor in the formation and imaging of the BSR at this location.

The relatively low saturation of hydrate estimated at the Blake Ridge, in addition to the homogeneity of the sediments, indicates that hydrate and free gas saturation are among the primary factors controlling the extensive, uninterrupted sections of the BSR at the Blake Ridge. The estimated hydrate and free gas concentrations at Terrebonne are higher than that at Blake Ridge, however, at these locations the lithology is the dominant factor in controlling the appearance of the BSR, as this in turn controls where the greatest accumulations of free gas occur, resulting in the appearance of a more distinct BSR in coarse grained units.

4.3 Orientation of seismic lines

The orientation of seismic lines relative to the geomorphology of hydrate bearing sediments may be a key factor in the imaging of a BSR where sediments are dipping. The seismic data set presented in this study at Blake Ridge, and used in previous work by Hornbach et al. (2008, 2003) and Gorman et al. (2002), is a pseudo-3D survey, resulting in relatively high-resolution imaging of sub-surface features. Due to this

pseudo-3D nature, however, only the inlines were used for mapping the BSR as the quality of the data in the crosslines is poor. Previous work published by Hornbach et al. (2008) shows that additional 2D seismic lines acquired roughly parallel to the crosslines of the pseudo-3D survey provide a clear image of the BSR (Hornbach et al. 2008 – their Fig. 6).

The BSR is most readily identified on seismic lines of one orientation; those that cross cut dipping sediments parallel to dip. At Terrebonne these are the crosslines (Fig. 4a), whereas at Orca the BSR is best imaged in the inlines (Fig. 6). It is harder to image the BSR on lines of the opposite orientation due to the sub-horizontal nature of the strata, particularly towards the center of these two basins.

At Blake Ridge, orientation of seismic lines is not a significant factor in imaging the BSR, which may be due to the sub-horizontal nature of the strata. Whereas at the Terrebonne and Orca sites where strata dip at 11-26°, highlighting the impact that seismic survey line orientation may have on the imaging of the BSR, in particular where strata are dipping. If the geomorphology of the strata is not understood prior to running the survey, it feasible that a BSR could be missed if the survey lines are oriented the wrong way. Whilst this is not an issue for 3D data, it is of concern for finer scale, 2D surveys where limited survey lines are acquired and not all intersection angles are covered.

4.4 Source Frequency

Seismic acquisition and the resultant resolution of the survey are a significant component in the imaging of a BSR, as demonstrated by Wood et al. (2008) and Chapman et al. (2002). Previous surveys at Blake Ridge utilized very high frequency data acquired with a deep-towed acoustic / geophysics system (DTAGS) (Wood et al., 2002; Wood and Gettrust, 2000). The DTAGS array is towed ~300 m above the seafloor, with source frequencies of 250-650 Hz, almost an order of magnitude higher than that of the conventional seismic data used in this location (Fig. 7) (Wood et al., 2002; Wood and Gettrust, 2000). The high-frequency source used in DTAGS produces seismic data with high vertical and lateral resolution, resulting in a very different image of the BSR with relation to the comparatively conventional

data used elsewhere. Seismic data at Blake Ridge published by Wood et al. (2002) (their Fig. 4c), shows that in the ultra-high-resolution DTAGS data, rather than being imaged as a cross cutting reflection, the BSR is characterized by a reflective zone of enhanced reflectivity, conformable with the strata. This is due to the decreased size of the Fresnel zone in the DTAGS data, allowing resolution of the strata containing free gas accumulations trapped below the hydrate bearing sediments (Chapman et al., 2002; Hyndman and Spence, 1992; Wood et al., 2002; Wood and Gettrust, 2000).

The availability of two seismic data sets at Terrebonne provides a valuable opportunity to compare and contrast the imaging of a BSR using seismic data acquired with different geometries and source frequencies. The conventional 3D seismic data set used in this study was recorded at a much lower source frequency in comparison to the high-resolution 2D seismic data set (Fig. 7), resulting in a much larger Fresnel zone. As shown in the results (Fig. 5), the BSR is stronger in the conventional 3D seismic data than in the high-resolution 2D seismic data due to the data acquisition parameters and seismic resolution. At Terrebonne the BSR resulting from focused accumulations of free gas in sands is clearly imaged as a coherent, discontinuous reflection in the 3D data, with a correspondingly large Fresnel zone, in contrast to the 2D data with a relatively small Fresnel zone.

At the Blake Ridge, the shallower depth to the BSR (~520 mbsf), and greater water depth (~2000-4000 m), in comparison to Terrebonne (~900 mbsf, 1500-2000 m), plays a significant role in the lateral resolution of the data, because the size of the Fresnel zone is partly dependent on the depth to the reflector. As a consequence, the BSR at the Blake Ridge is averaged over a greater lateral area, which increases amplitude and lateral continuity of the reflection, particularly for the pseudo-3D data. As discussed by Wood et al. (2008), the BSR at Blake Ridge is more clearly imaged as a cross cutting reflection using high-resolution 2D data, rather than the ultra-high-resolution DTAGS data. The DTAGS data, however, shows the stratigraphic and lithologic disposition of hydrate in these sediments with more detail due to the decreased Fresnel zone size and increased lateral resolution of the data.

The conventional 3D seismic data at Orca Basin have a similar source frequency to the conventional 3D seismic data at Terrebonne (Fig. 4), and as at Terrebonne, the BSR is resolved as a clear and distinct reflection. In addition, the 2D seismic data at Orca Basin have a similar source frequency to the conventional 3D data, and the BSR is readily identifiable in these data as well (Fig. 6b). As there is no high-resolution seismic data available at this site, we cannot compare this to a higher source frequency data set. However, based on the geological similarities to Terrebonne, high-resolution seismic data at Orca would likely clarify the finer details of the BGHSZ.

Guerin et al. (1999) and Holbrook et al. (1996) proposed that the BSR represents the first appearance of free gas, rather than the transition from gas hydrate to free gas. At Terrebonne and Orca Basin, the conventional 3D data suggest the BSR is a discrete reflection; the high-resolution 2D data, however, indicate that the BSR may occur in the transition zone from hydrate to free gas, being resolved into a series of discontinuous reflections in the high-resolution seismic image (Fig. 8). As shown in Fig. 5, it is possible to identify the BSR in the high-resolution 2D data at Terrebonne; however, the BSR is no longer characterized as a cross-cutting reflection. Rather, it can be identified as the uppermost extent of enhanced amplitude negative polarity strata.

Through examining extensive data sets with variable source frequencies, and resultant resolutions, we demonstrate the significant impact of source frequency on the imaging of BSRs. Even the textbook continuous BSR at Blake Ridge becomes fragmented across the extent of the pseudo-3D data set, and when imaged using ultra-high resolution DTAGS data, is shown to be discontinuous. Similarly, at Terrebonne, high resolution 2D data reveals the BSR as increasingly inconsistent in comparison to the lower resolution conventional 3D data.

4.5 Summary of discussion

The key points of the discussion are summarized in Table 1. The data presented in this study highlight the multitude of interlinked factors that influence the formation and imaging of BSRs in seismic data. Based

on these observations, conventional seismic methods are useful to determine the regional distribution of the BSR and associated gas hydrate anomaly zones. More detailed, high-resolution seismic methods are useful in local hydrate studies that follow conventional seismic acquisition, or in advance of drilling, as this provides critical details about the BSR morphology, BSR patterns, and other geological features within the hydrate stability field. The differences in seismic image resolution complement one another well and are especially useful in target areas for exploration (production) drilling as well as for research (landslide, fluid flow, volume) studies.

Table 1: Summary of factors influencing the formation and imaging of the BSR in the two regions presented in this paper.

	Blake Ridge	***Gulf of Mexico (Terrebonne and Orca Basins)***
Formation characteristics	Homogeneous lithology has limited control on BSR formation.	Heterogeneous lithology of interbedded muds and sands has significant impact on BSR formation. Primary physical control factor.
Gas hydrate & free gas occurrence	Low saturation required to produce significant acoustic impedance, therefore is a primary control on BSR formation. Main physical control factor.	Variable saturation (controlled by lithology), plays a significant role in BSR formation, but is linked primarily to formation characteristics. Secondary control factor.
Orientation of seismic lines	Sub-horizontal strata results in limited impact of line orientation on imaging of the BSR.	Uniformly dipping strata results in significant impact of line orientation on how the BSR is imaged.
Source frequency	High resolution pseudo-3D data – imaged as a continuous BSR across much of the area, but fragmented across wider extent. Ultra-high resolution DTAGS data – imaged as a discontinuous BSR.	Low resolution 3D data and 2D data – imaged as a fragmented, discontinuous BSR. High resolution 2D data (Terrebonne) – BSR further disintegrates into a patchy, inconsistent feature.

Conclusions

We use seismic data of varying source frequencies to precisely map BSRs in 3D at three locations, highlighting the impact of heterogeneous lithology and geomorphology on controlling the distribution of gas hydrate and free gas. We find that acquisition geometry and source frequency are critical factors for

interpreting BSRs imaged in marine sediments, and therefore, are fundamental controls on characterizing the presence of gas hydrates from seismic data.

We argue that all BSRs are in fact discontinuous in nature; however, whether they are imaged as such, depends on the resolution of the seismic data. Provided that there are high enough resolution seismic data to resolve the strata containing the BSR, the BSR will be resolved as an upper extent of reflective sediments below the base of gas hydrate stability, rather than an unconformable, cross-cutting reflection. As a result, the acquisition geometry and resolution of seismic data becomes a principle factor in imaging BSRs and characterizing gas hydrates. This is particularly significant in a complex setting where numerous other elements, such as lithology and free gas saturation, play a role in the formation of a BSR. This may help to explain why we occasionally encounter hydrates in areas where a BSR has not been identified in seismic data.

Acknowledgments

This material is based upon work supported by the Department of Energy under Award Number DE-FE0023919. The Blake Ridge data were acquired as part of the project: Three-Dimensional Structure and Physical Properties of a Methane Hydrate Deposit and Methane Gas Reservoir, Blake Ridge, and funding was provided by NSF grant: OCE99-10966. These data were made available through the UTIG Academic Seismic Portal. The 2D data at Terrebonne and Orca Basin were made available through the USGS National Archive of Marine Seismic Surveys. This paper benefited greatly from significant comments by Seth Haines, and revisions by Warren Wood and an anonymous reviewer. HMK acknowledges support from Tubitak for the analyses performed in this research.

Disclaimer

completeness, or usefulness of any information, apparatus, product, or process disclosed, or represents that its use would not infringe privately owned rights. Reference herein to any specific commercial product, process, or service by trade name, trademark, manufacturer, or otherwise does not necessarily constitute or imply its endorsement, recommendation, or favoring by the United States Government or any agency thereof. The views and opinions of authors expressed herein do not necessarily state or reflect those of the United States Government or any agency thereof."

References

Andreassen, K., Hart, P.E., Grantz, A., 1995. Seismic studies of a bottom simulating reflection related to gas hydrate beneath the continental margin of the Beaufort Sea. J. Geophys. Res. 100, 12659. doi:10.1029/95JB00961

Berndt, C., Bünz, S., Clayton, T., Mienert, J., Saunders, M., 2004. Seismic character of bottom simulating reflectors: examples from the mid-Norwegian margin. Mar. Pet. Geol. 21, 723–733. doi:10.1016/j.marpetgeo.2004.02.003

Boswell, R., Collett, T.S., Frye, M., Shedd, W., McConnell, D.R., Shelander, D., 2012a. Subsurface gas hydrates in the northern Gulf of Mexico. Mar. Pet. Geol. 34, 4–30. doi:10.1016/j.marpetgeo.2011.10.003

Boswell, R., Frye, M., Shelander, D., Shedd, W., McConnell, D.R., Cook, A., 2012b. Architecture of gas-hydrate-bearing sands from Walker Ridge 313, Green Canyon 955, and Alaminos Canyon 21: Northern deepwater Gulf of Mexico. Mar. Pet. Geol. 34, 134–149. doi:10.1016/j.marpetgeo.2011.08.010

Bryan, G.M., 1974. In Situ Indications of Gas Hydrate, in: Kaplan, I.R. (Ed.), Natural Gases in Marine Sediments. Springer USA, New York, USA, pp. 299–308. doi:10.1007/978-1-4684-2757-8_17

Bulat, J., 2005. Some considerations on the interpretation of seabed images based on commercial 3D seismic in the Faroe-Shetland Channel. Basin Res. 17, 21–42. doi:10.1111/j.1365-

2117.2005.00253.x

Bünz, S., Mienert, J., Berndt, C., 2003. Geological controls on the Storegga gas-hydrate system of the mid-Norwegian continental margin. Earth Planet. Sci. Lett. 209, 291–307.

Chapman, N.R., Gettrust, J.F., Walia, R., Hannay, D., Spence, G.D., Wood, W.T., Hyndman, R.D., 2002. High resolution, deep towed, multichannel seismic survey of deep sea gas hydrates off western Canada. GEOPHYSICS 67, 1038–1047. doi:10.1190/1.1500364

Clennell, M.B., Henry, P., Hovland, M., Booth, J.S., Winters, G.J., Thomas, M., 2000. Formation of natural gas hydrates in marine sediments: Gas hydrate growth and stability conditioned by host sediment properties. Gas Hydrates Challenges Futur. 912, 887–896.

Clennell, M. Ben, Hovland, M., Booth, J.S., Henry, P., Winters, W.J., 1999. Formation of natural gas hydrates in marine sediments: 1. Conceptual model of gas hydrate growth conditioned by host sediment properties. J. Geophys. Res. Solid Earth 104, 22985–23003. doi:10.1029/1999JB900175

Cook, A.E., Goldberg, D.S., Malinverno, A., 2014. Natural gas hydrates occupying fractures: A focus on non-vent sites on the Indian continental margin and the northern Gulf of Mexico. Mar. Pet. Geol. 58, 278–291. doi:10.1016/j.marpetgeo.2014.04.013

Daigle, H., Dugan, B., 2014. Pore size controls on the base of the methane hydrate stability zone in the Kumano Basin, offshore Japan. Geophys. Res. Lett. 41, 8021–8028. doi:10.1002/2014GL062135

Davies, R.J., Cartwright, J., 2002. A fossilized Opal A to Opal C/T transformation on the northeast Atlantic margin: support for a significantly elevated Palaeogeothermal gradient during the Neogene? Basin Res. 14, 467–486. doi:10.1046/j.1365-2117.2002.00184.x

Diegel, F.A., Karlo, J.F., Schuster, D.C., Shoup, R.C., Tauvers, P.R., 1995. Cenozoic Structural Evolution and Tectono-Stratigraphic Framework of the Northern Gulf Coast Continental Margin, in: Jackson, M.P.A., Roberts, D.G., Snelson, S. (Eds.), Salt Tectonics: A Global Perspective: AAPG Memoir 65. AAPG, pp. 109–151.

Ecker, C., Dvorkin, J., Nur, A.M., 2000. Estimating the amount of gas hydrate and free gas from marine seismic data. GEOPHYSICS 65, 565–573. doi:10.1190/1.1444752

Frye, M., Shedd, W., Boswell, R., 2012. Gas hydrate resource potential in the Terrebonne Basin, Northern Gulf of Mexico. Mar. Pet. Geol. 34, 150–168. doi:10.1016/j.marpetgeo.2011.08.001

Goldberg, D.S., Wilkins, R.H., Moos, D., 1987. Seismic modeling of diagenetic effects in cenozoic marine sediments. Init. Repts. Deep Sea Drilling Project, 95. US Government Printing Office, Washington, DC, USA.

Gorman, A.R., Holbrook, W.S., Hornbach, M.J., Hackwith, K.L., Lizarralde, D., Pecher, I., 2002. Migration of methane gas through the hydrate stability zone in a low-flux hydrate province. Geology 30, 327–330.

Guerin, G., Goldberg, D., Meltser, A., 1999. Characterization of in situ elastic properties of gas hydrate-bearing sediments on the Blake Ridge. J. Geophys. Res. 104, 17781–17795.

Haacke, R.R., Westbrook, G.K., Hyndman, R.D., 2007. Gas hydrate, fluid flow and free gas: Formation of the bottom-simulating reflector. Earth Planet. Sci. Lett. 261, 407–420.

Haines, S.S., Hart, P.E., Ruppel, C., O'Brien, T., Baldwin, W., White, J., Moore, E., Dal Ferro, P., Lemmond, P., 2014. Cruise Report for P1–13–LA, U.S. Geological Survey Gas Hydrates Research Cruise, R/V Pelican April 18 to May 3, 2013, Deepwater Gulf of Mexico.

Holbrook, W.S., Gorman, A.R., Hornbach, M.J., Hackwith, K.L., Nealon, J., Lizarralde, D., Pecher, I., 2002. Seismic detection of marine methane hydrate. Lead. Edge 686–689.

Holbrook, W.S., Hoskins, H., Wood, W.T., Stephen, R.A., Lizarralde, D., 1996. Methane hydrate and free gas on the Blake Ridge from vertical seismic profiling. Science (80-.). 273, 1840–1843.

Hornbach, M.J., Holbrook, W.S., Gorman, A.R., Hackwith, K.L., Lizarralde, D., Pecher, I.A., 2003. Direct seismic detection of methane hydrate on the Blake Ridge. Geophysics 68, 92–100.

Hornbach, M.J., Saffer, D., Holbrook, W.S., Van Avendonk, H., Gorman, A.R., 2008. Three-dimensional

seismic imaging of the Blake Ridge methane hydrate province: Evidence for large, concentrated zones of gas hydrate and morphologically driven advection. J. Geophys. Res. 113.

Hyndman, R.D., Spence, G.D., 1992. A seismic study of methane hydrate marine bottom simulating reflectors. J. Geophys. Res. 97, 6683. doi:10.1029/92JB00234

Janos, D., Zhang, D., 2012. Data Processing Report: Walker Ridge / Keathley Canyon Wide Azimuth 3-D Q-Marine "E-Octopus Phase VII." Houston, Texas, USA.

Lee, G.H., Kim, H.-J., Jou, H.-T., Cho, H.-M., 2003. Opal-A/opal-CT phase boundary inferred from bottom-simulating reflectors in the southern South Korea Plateau, East Sea (Sea of Japan). Geophys. Res. Lett. 30. doi:10.1029/2003GL018670

Lee, M.W., Hutchinson, D.R., Agena, W.F., Dillon, W.P., Miller, J.J., Swift, B.A., 1994. Seismic character of gas hydrates on the Southeastern U.S. continental margin. Mar. Geophys. Res. 16, 163–184. doi:10.1007/BF01237512

Liu, X., Flemings, P.B., 2007. Dynamic multiphase flow model of hydrate formation in marine sediments. J. Geophys. Res. 112, B03101. doi:10.1029/2005JB004227

Majumdar, U., Cook, A.E., Shedd, W., Frye, M., 2016. The connection between natural gas hydrate and bottom-simulating reflectors. Geophys. Res. Lett. 43, 7044–7051. doi:10.1002/2016GL069443

Markl, R.G., Bryan, G.M., Ewing, J.I., 1970. Structure of the Blake-Bahama Outer Ridge. J. Geophys. Res. 75, 4539–4555. doi:10.1029/JC075i024p04539

Max, M.D., Dillon, W.P., 1998. Oceanic methane hydrate: the character of the Blake Ridge hydrate stability zone, and the potential for methane extraction. J. Pet. Geol. 21, 343–358. doi:10.1111/j.1747-5457.1998.tb00786.x

McConnell, D.R., Kendall, B.A., 2013. Images of the Base of Gas Hydrate Stability, Northwest Walker Ridge, Gulf of Mexico, in: Offshore Technology Conference. Offshore Technology Conference. doi:10.4043/14103-MS

550 Murphy, W., Reischer, A., Hsu, K., 1993. Modulus decomposition of compressional and shear velocities
551 in sand bodies. Geophysics 58, 227–239.

552 Paganoni, M., Cartwright, J.A., Foschi, M., Shipp, R.C., Van Rensbergen, P., 2016. Structure II gas
553 hydrates found below the bottom-simulating reflector. Geophys. Res. Lett. 43, 5696–5706.
554 doi:10.1002/2016GL069452

555 Paull, C.K., Wallace, P.J., Scientific Shipboard Party, 1996. Proceedings of the Ocean Drilling Program,
556 Scientific Results. Proc. Ocean Drill. Program, Initial Reports 164.

557 Petersen, C.J., Papenberg, C., Klaeschen, D., 2007. Local seismic quantification of gas hydrates and BSR
558 characterization from multi-frequency OBS data at northern Hydrate Ridge. Earth Planet. Sci. Lett.
559 255, 414–431. doi:10.1016/j.epsl.2007.01.002

560 Pilcher, R.S., Blumstein, R.D., 2007. Brine volume and salt dissolution rates in Orca Basin, northeast
561 Gulf of Mexico. Am. Assoc. Pet. Geol. Bull. 91, 823–833.

562 Shedd, W., Boswell, R., Frye, M., Godfriaux, P., Kramer, K., 2012. Occurrence and nature of “bottom
563 simulating reflectors” in the northern Gulf of Mexico. Mar. Pet. Geol. 34, 31–40.

564 Shipley, T.H., Houston, M.H., Buffler, R.T., Shaub, F.J., McMillen, K.J., Ladd, J.W., Worzel, J.L., 1979.
565 Seismic Evidence for Widespread Possible Gas Hydrate Horizons on Continental Slopes and Rises.
566 Am. Assoc. Pet. Geol. Bull. 63, 2204–2213.

567 Triezenberg, P.J., Hart, P.E., Childs, J.R., 2016. National Archive of Marine Seismic Surveys (NAMSS):
568 A USGS Data Website of marine seismic reflection data within the U.S. Exclusive Economic Zone
569 (EEZ): U.S. Geological Survey Data Release. doi:10.5066/F7930R7P

570 Waughman, D., O’Connor, J., 2007. Final Field Operation Report Marine Seismic Reflection Survey:
571 Multiclient E-Octopus Phase II WAZ. Houston, Texas, USA.

572 Westbrook, G.K., Buenz, S., Camerlenghi, A., Carcione, J., Chand, S., Dean, S., Foucher, J.P., Flueh, E.,
573 Gei, D., Haacke, R., Klingelhoefer, F., Long, C., Madrussani, G., Mienert, J., Minshull, T.A.,

574 Nouzé, H., Peacock, S., Rossi, G., Roux, E., Reston, T., Vanneste, M., Zillmer, M., 2005.
575 Measurement of P- and S-wave Velocities, and the Estimation of Hydrate Concentration at Sites in
576 the Continental Margin of Svalbard and the Storegga Region of Norway., in: Proceedings of the 5th
577 International Conference on Gas Hydrates, Vol. 3. pp. 726–735.

578 Wood, W.T., Gettrust, J.F., 2000. Deep tow Seismic Investigations of Methane Hydrates, in: Paull, C.K.,
579 Dillon, W.P. (Eds.), AGU Monograph Series: Natural Gas Hydrates: Occurrence, Distribution, and
580 Dynamics. American Geophysical Union, pp. 656–660. doi:10.1029/GM124p016

581 Wood, W.T., Gettrust, J.F., Chapman, N.R., Spence, G.D., Hyndman, R.D., 2002. Decreased stability of
582 methane hydrates in marine sediments owing to phase-boundary roughness. Nature 420, 656–60.
583 doi:10.1038/nature01263

584 Wood, W.T., Hart, P.E., Hutchinson, D.R., Dutta, N., Snyder, F., Coffin, R.B., Gettrust, J.F., 2008. Gas
585 and gas hydrate distribution around seafloor seeps in Mississippi Canyon, Northern Gulf of Mexico,
586 using multi-resolution seismic imagery. Mar. Pet. Geol. 25, 952–959.
587 doi:10.1016/j.marpetgeo.2008.01.015

588 Worrall, D.M., Snelson, S., 1989. Evolution of the northern Gulf of Mexico, with emphasis on Cenozoic
589 growth faulting and the role of salt, in: Bally, A.W., Palmer, A.R. (Eds.), The Geology of North
590 America - An Overview. Geological Society of America, Boulder, Colorado, pp. 97–138.

591 Xu, W., Ruppel, C., 1999. Predicting the occurrence, distribution, and evolution of methane gas hydrate
592 in porous marine sediments. J. Geophys. Res. Solid Earth 104, 5081–5095.
593 doi:10.1029/1998JB900092

594 Yilmaz, Ö., 2001. Seismic Data Analysis: Processing, inversion, and interpretation of seismic data.
595 Society of Exploration Geophysicists. doi:10.1190/1.9781560801580

596

597

598 **Figures:**

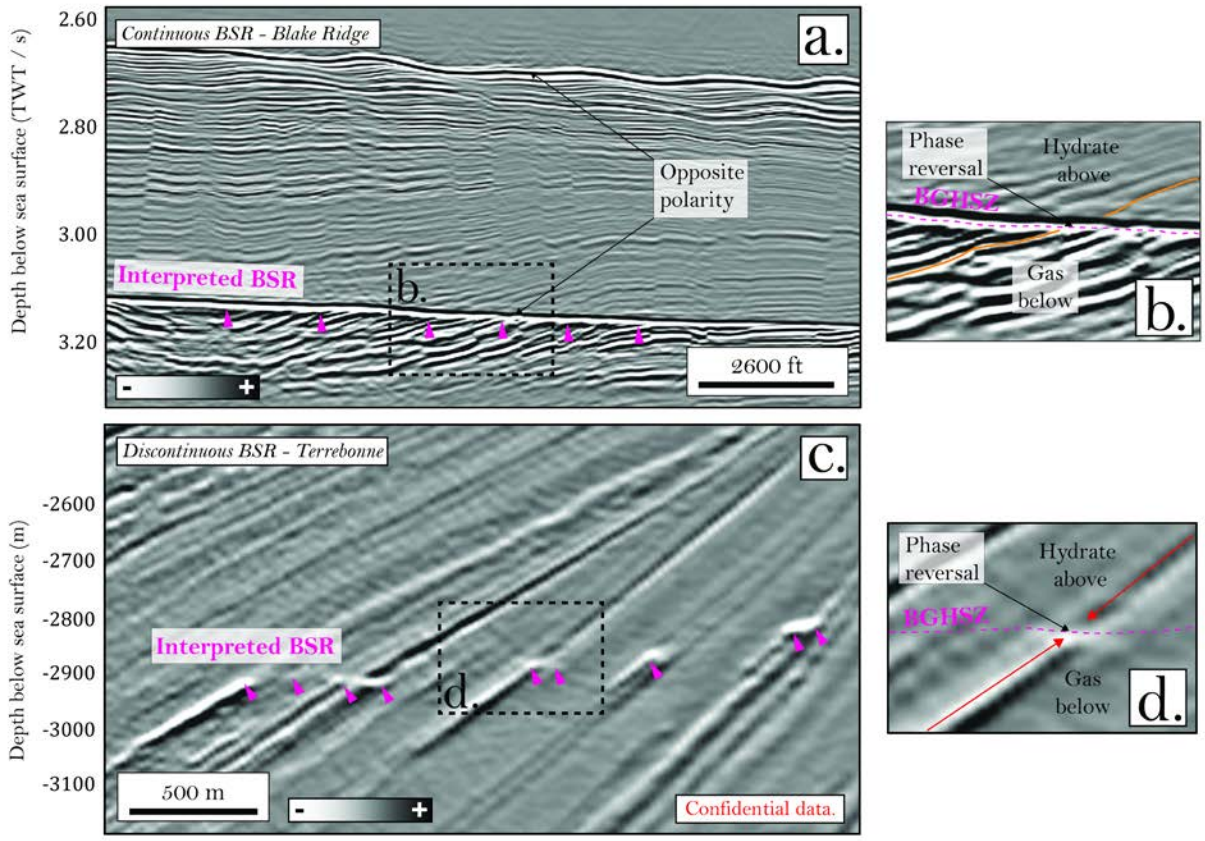

599

600 **Fig. 1** Examples of continuous and discontinuous bottom simulating reflections (BSRs). (a) Continuous
601 BSR at Blake Ridge. The BSR is clearly distinguished as a laterally continuous reflection following the
602 geomorphology of the seafloor, with opposite polarity to the seafloor. (b) Enlarged section of (a) to show
603 phase reversal at the BSR of the horizon marked in orange. (c) Discontinuous BSR at Terrebonne. The
604 BSR is distinguished by spaced negative polarity events. (d) Enlarged section of (c) showing polarity
605 reversal at BSR of the horizon marked in red.

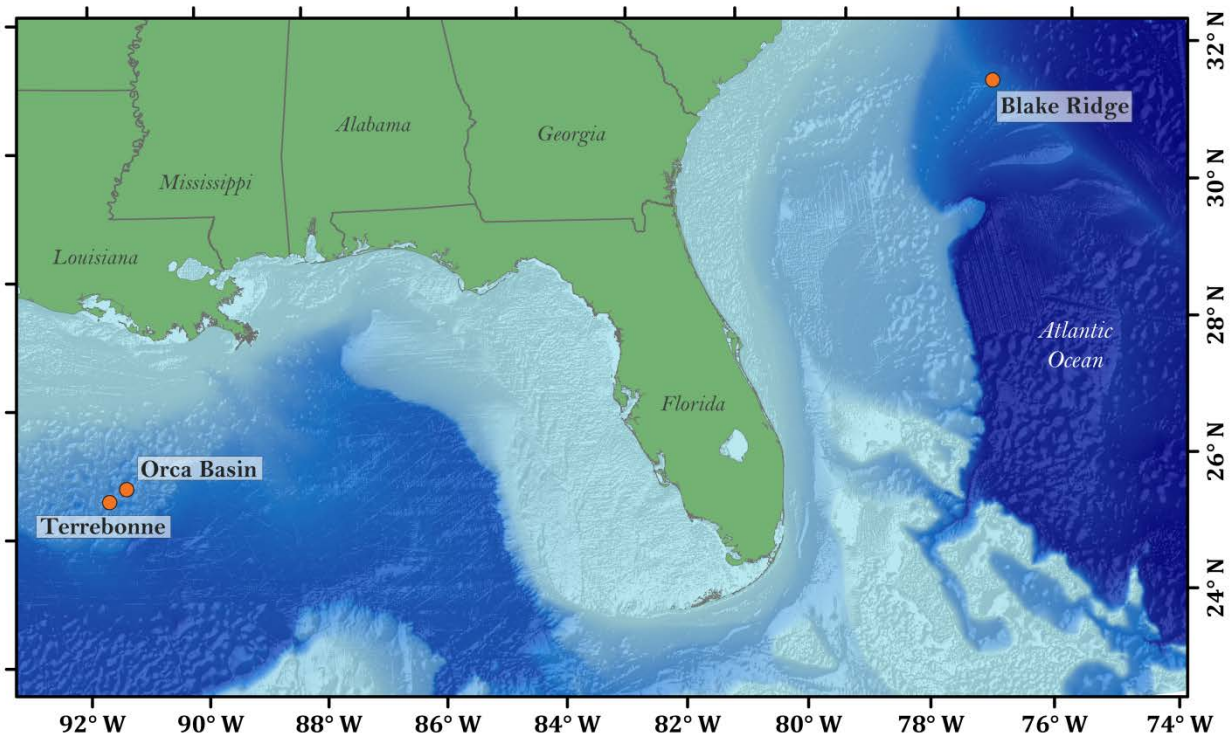

606

607 **Fig. 2** Map to show the location of the study areas in the Gulf of Mexico and the Atlantic Ocean.

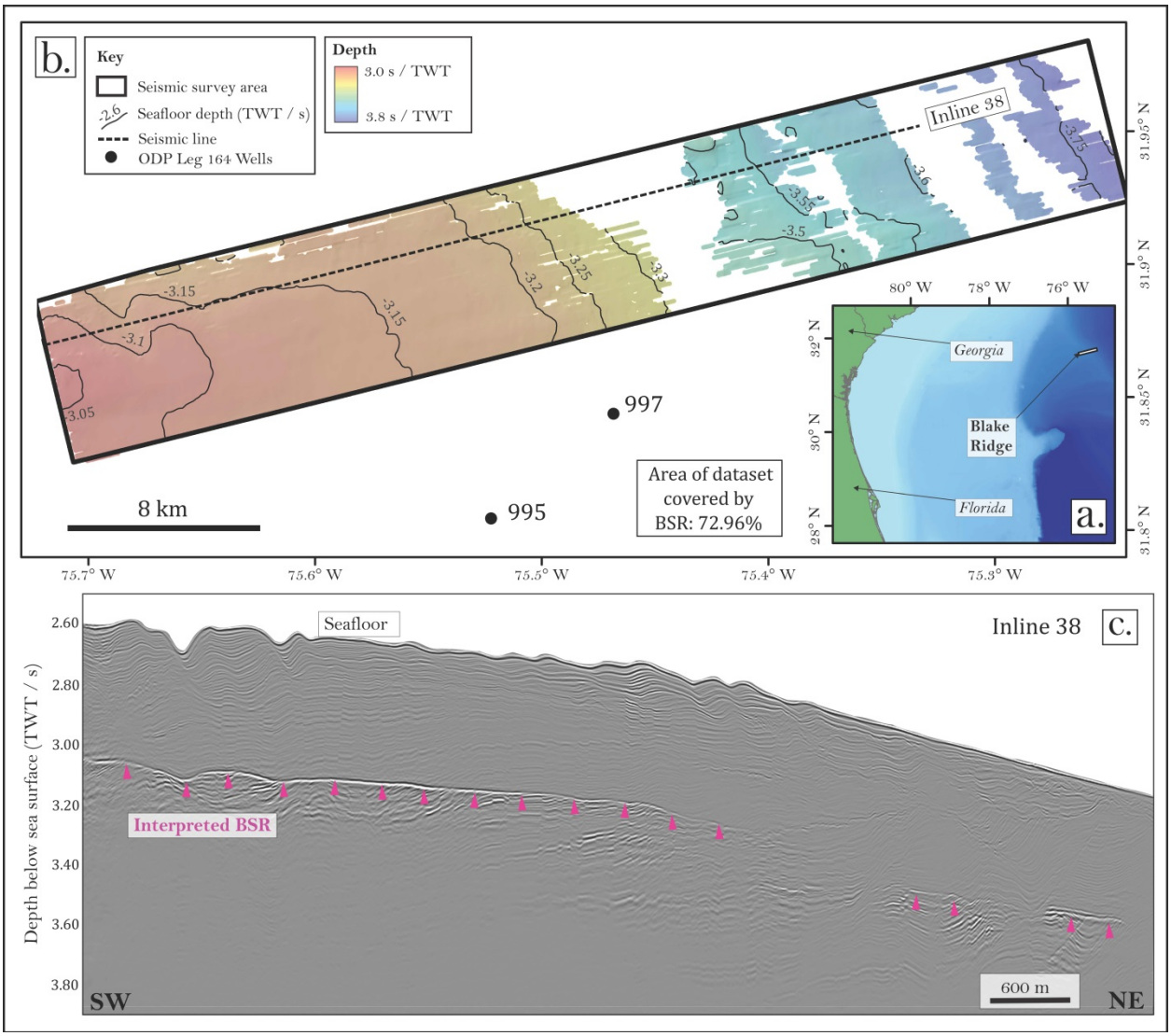

Fig. 3 (a) Location of the Blake Ridge survey area. (b) Structural map of the BSR at Blake Ridge. (c) Inline 38 from 3D seismic data showing the continuous nature of the BSR in the western section of the area. To the east the BSR deteriorates into a more discontinuous BSR. The mapped BSR covers 72.96% of the data set area. Data source: USGS.

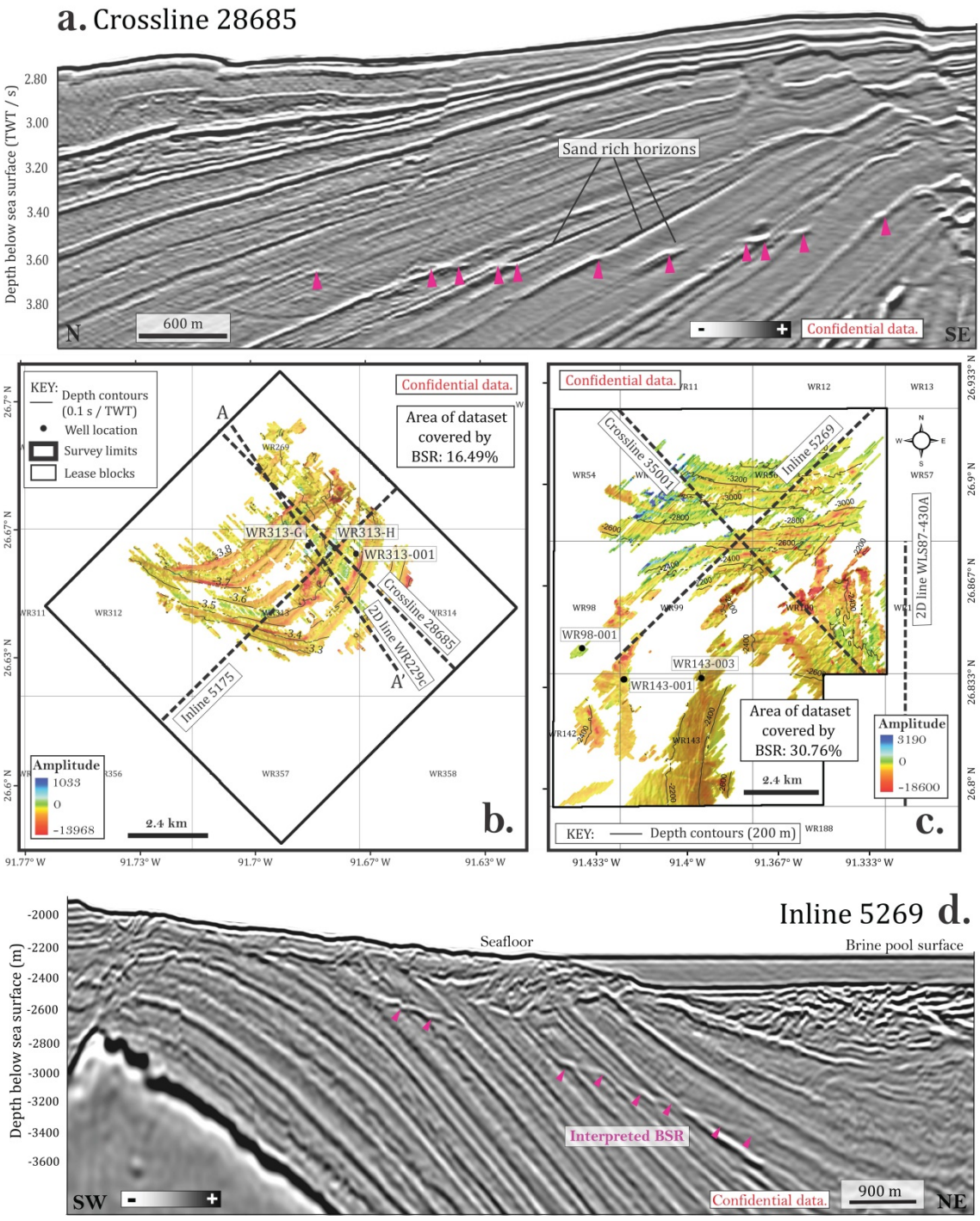

Fig. 4 (a) Seismic profile (Crossline 28685) showing the typical characteristics of the BSR in 3D conventional data at Terrebonne. Position of Crossline 28685 as shown in (b) below. (b) Amplitude map of the BSR at Terrebonne. Note the high amplitude stripes correlating to the position of coarse grained sand units. The mapped BSR covers 16.49% of the data set area. (c) Amplitude map of the BSR at Orca

618 Basin. The mapped BSR covers 30.76% of the data set area. The locations of existing well sites are
619 indicated on the maps, as are the locations of seismic lines included in this study. (d) Seismic profile
620 (Inline 5269) showing the typical characteristics of the BSR in 3D conventional data at Orca Basin.
621 Position of Inline 5269 as shown in (c) above.

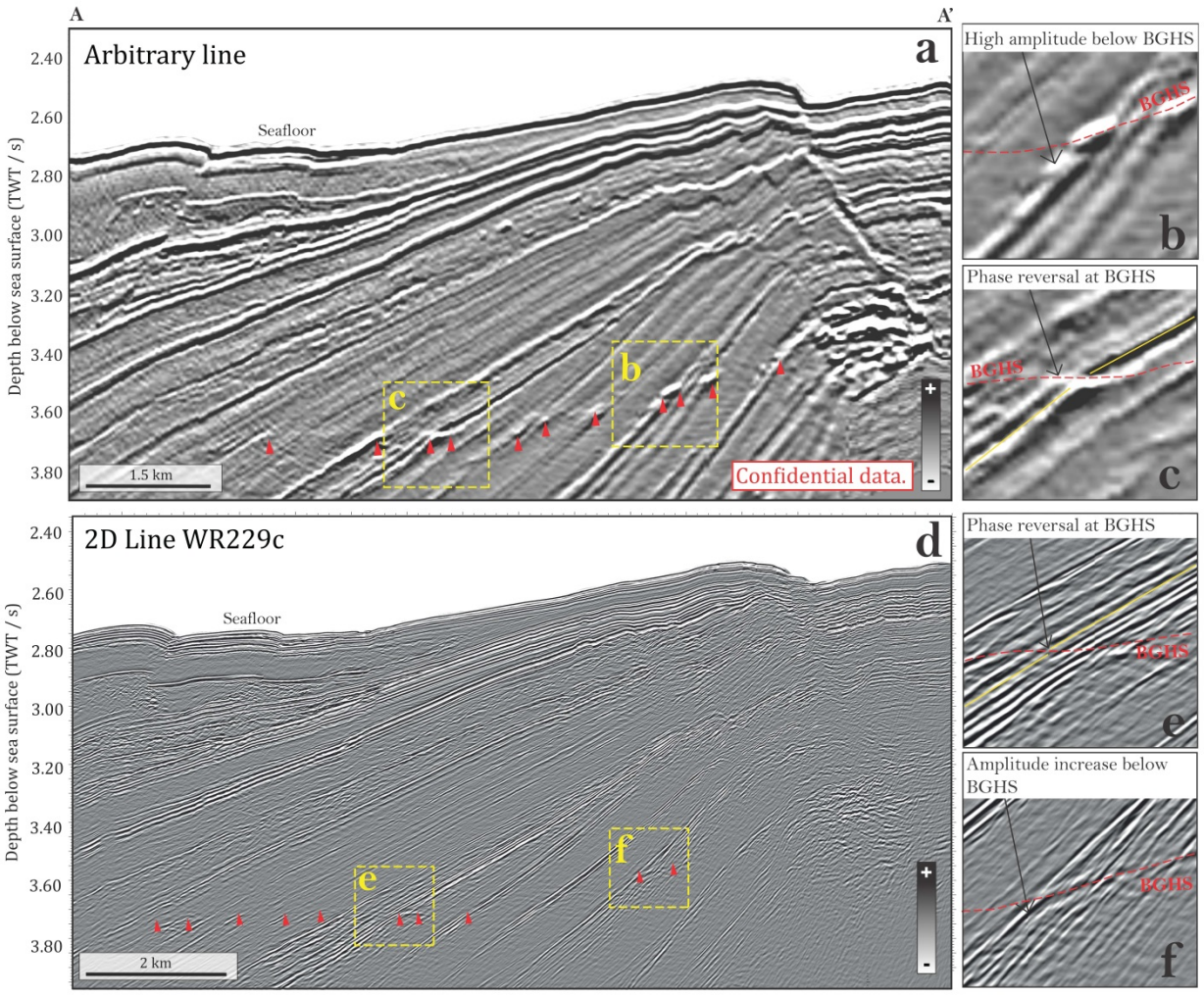

622

623 **Fig. 5** Comparison of a bottom simulating reflection (BSR) imaged in conventional 3D and high-
624 resolution 2D data at Terrebonne. (a) Arbitrary 3D seismic line along same path as 2D line WR229c. The
625 minor vertical artifacts in the seismic data are due to this being an arbitrary line drawn across the 3D
626 volume. The BSR is clearly defined by spaced, high amplitude reflections where the BSR crosses dipping
627 sand units (indicated by red arrows). These units are associated with increased amplitudes below the BSR

(b) and phase reversal as they cross the BSR (c). The base of gas hydrate stability (BGHS) is indicated by a red dashed line. (d) 2D prestack Kirchoff time migration of the 2D high-resolution data, line WR229c, for line location see Fig. 4b. In contrast to the 3D data, the BSR is less apparent; however, finer details of the sedimentary strata are visible and the BSR can be traced. As with the 3D data, the BSR is characterized by phase reversal of dipping sand units (e) and increased amplitudes below the BSR (f).

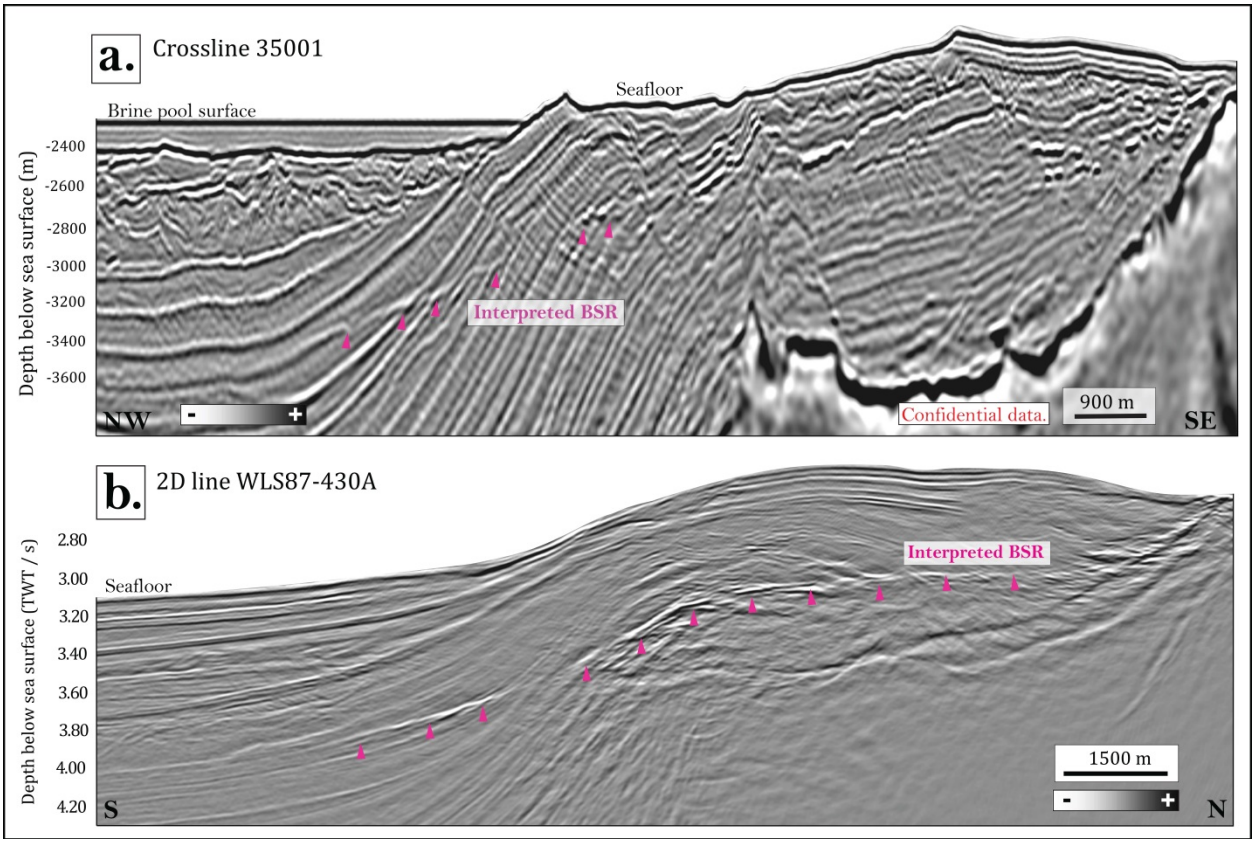

Fig. 6 Comparison of a bottom simulating reflection (BSR) imaged in 3D and 2D data at the Orca Basin. (a) Crossline 35001. The BSR is identifiable as a discontinuous, patchy reflection. (c) 2D seismic line WLS87-430A. The BSR is visible as a faint, negative amplitude reflection that can be traced laterally across the section. For location of seismic lines, see Fig. 4c.

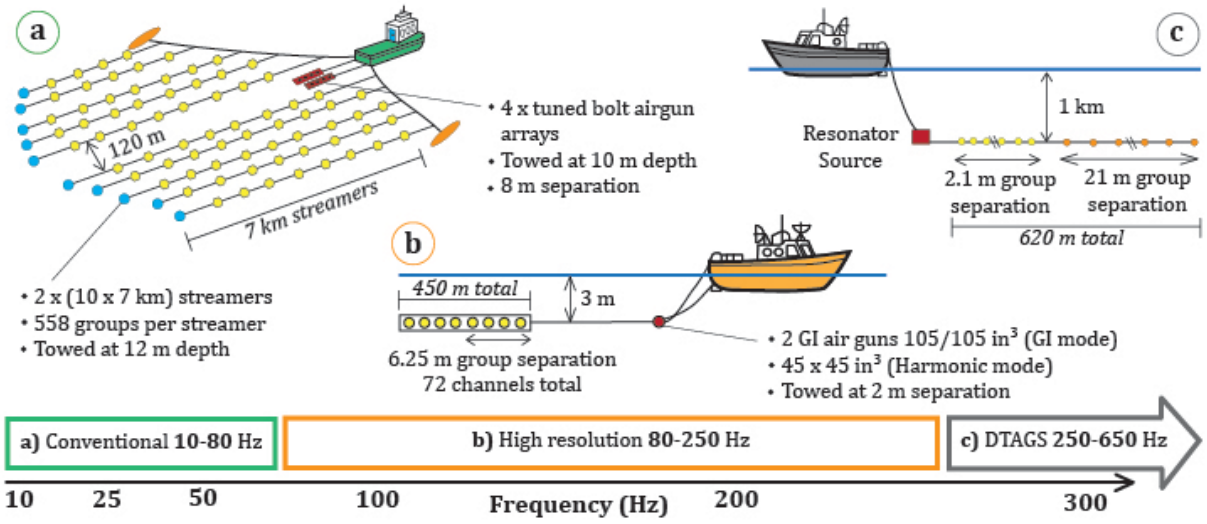

638

639 **Fig. 7** Schematic diagram to show the variation in acquisition systems and frequency content of the
640 different seismic data types discussed here. (a) Conventional seismic survey, parameters detailed here are
641 those used in the acquisition of 3D conventional data at Terrebonne. (b) High-resolution seismic survey,
642 parameters detailed here are those used in the acquisition of 2D data at Terrebonne. (c) DTAGS system
643 used to acquire ultra-high-resolution, after Chapman et al. (2002).

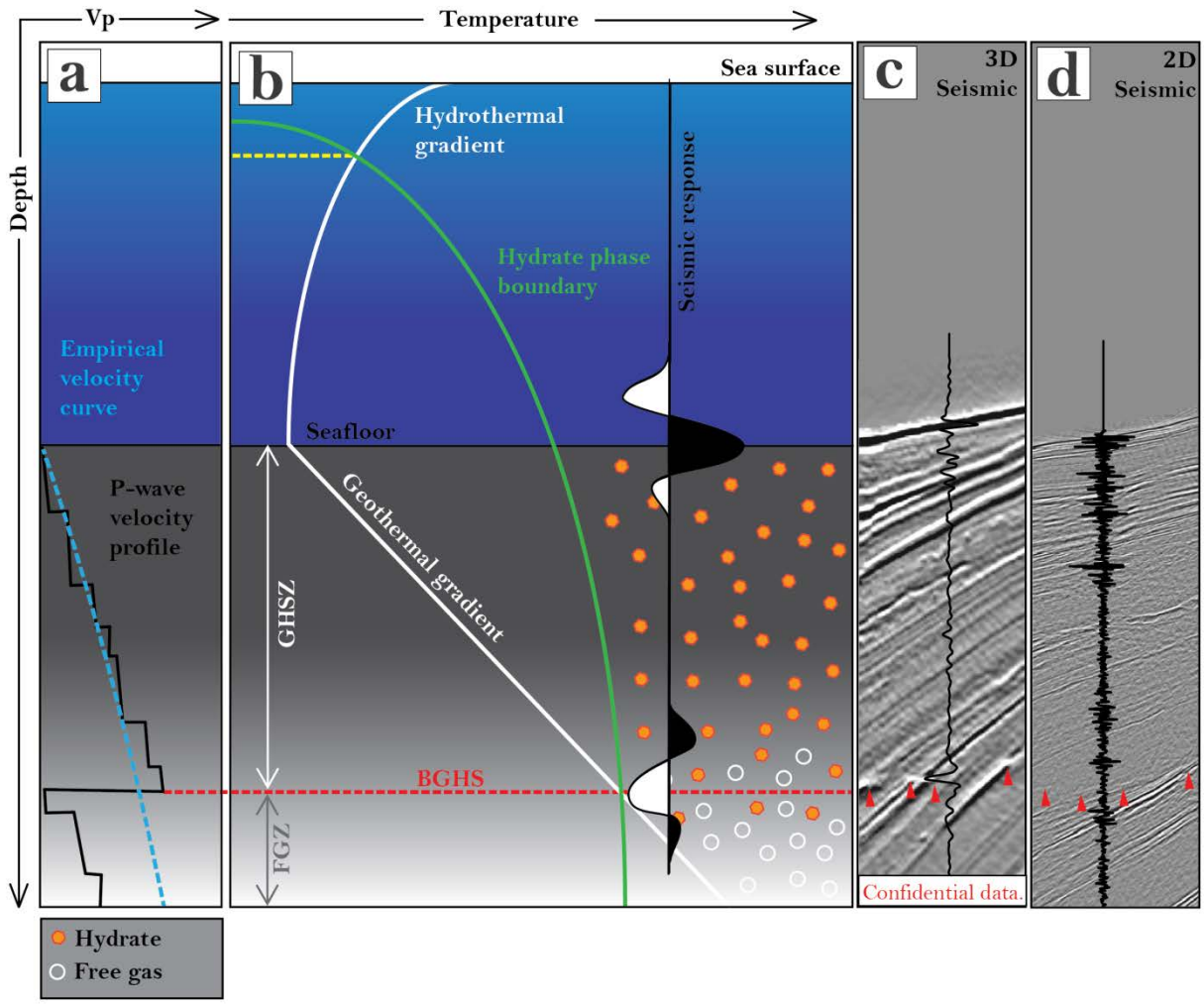

644

645 **Fig. 8** Schematic diagram to show the impact of different seismic frequencies when imaging a BSR. (a)
646 P-wave velocity curve (black) from a site west of Svalbard (Westbrook et al., 2005), indicating a thick
647 sub-BSR free gas zone (FGZ) with a downward decreasing concentration of free gas. In comparison, the
648 dashed blue line is an empirical velocity curve for soft terrigenous muds. (b) Illustration of a submarine
649 sedimentary section containing gas hydrate (above) and free gas (below) the base of gas hydrate stability
650 (BGHS). This reflector denotes the base of the gas hydrate stability zone (GHSZ) (after Haacke et al.,
651 2007). (c) Section of a 3D seismic line at Terrebonne, seismic trace overlaid. (d) Section of a 2D seismic
652 line at Terrebonne, seismic trace overlaid. The position of the interpreted BSR is indicated by red
653 triangles.

Appendix A: Acquisition details for seismic data.

Table A.1 Summary of seismic data acquisition (Gorman et al., 2002; Haines et al., 2014; Holbrook et al., 2002; Hornbach et al., 2008, 2003; Janos and Zhang, 2012; Triezenberg et al., 2016; Waughman and O'Connor, 2007).

Survey Area	*Date*	*Type*	*Vessel(s)*	*Source*	*Receiver*
Terrebonne	2006-2007	*3D*	*M/V Western Neptune, M/V Ocean Odyssey, M/V Geco Tau and M/V Western Regent*	4 Tuned Bolt airgun arrays, comprised of 5 sub-arrays per array, 8 guns per sub-array at 8 m separation. Configured at 8475 in^3 per array. Towed at 10 m below sea surface with 8 m separation. Shot interval 37.5 m.	2 x (10 x 7 km) streamers, 120 m separation between streamers, 558 groups per streamer, towed at 12 m below sea surface. Sample rate 2 ms.
	2013	*2D**	*R/V Pelican*	2 GI air guns, configured at 105/105 in^3 (harmonic mode) or 45/45 in^3 (GI mode), with a separation of 2 m, towed at a depth of 3 m. Shot interval of 25 s in harmonic mode, 10 s in GI mode.	Geometrics GeoEel oil-filled digital hydrophone streamer. Nine 50 m sections, each with 8 channels at 6.25 m group spacing (72 channels total). Towed at a depth of 3 m.
Orca Basin	2009-2010	*3D*	*WG Columbus, M/V Western Regent, M/V Western Snapper, M/V Geco Tau and M/V Ocean Odyssey*	4 Tuned Bolt airgun arrays, comprised of 5 sub-arrays per array, 8 guns per sub-array at 8 m separation. Configured at 8475 in^3 per array. Towed at 10 m below sea surface with 8 m separation. Shot interval 37.5 m.	10 x 7 km streamers, 120 m separation between streamers, 558 groups per streamer, 12.5 m group interval, towed at 12 m below sea surface.
	1987	*2D*	*WesternGeco*	Airgun source.	24 channel streamer.
Blake Ridge	2000	*2D / 3D*	*R/V Maurice Ewing*	2 high frequency GI air guns, configured at 105/105 in^3. Towed at 5 m below sea surface, shot spacing of 37.5 m.	4 km streamer, 324 channels grouped in 12.5 m intervals, towed at 5 m below sea surface at 5 knots.

* Note: 2D high-resolution seismic data were collected aboard R/V Pelican (Haines et al., 2014). A

global DGPS and navigation system was utilized during expedition. A 450 m-long digital streamer with 6.25 m group spacing was used to acquire seismic data. Data were collected with various record length up to 10 s for different profiles and the sample rate was 0.5 ms. An air gun array including two Generator-Injector (GI) type air guns was used as an energy source in harmonic mode (105+105 or 45+45 cubic inches) which has generated sharp signal between 10 – 300 Hz frequency band. Air guns were simultaneously fired at every 25 sec. for 105+105 in^3 mode and at every 10 sec. for 45+45 in^3 mode along different profiles. The streamer was towed 3 m below sea surface using GeoSpace bird depth controllers, the gun array was also towed at 3 m.

Appendix B: Processing of the high-resolution 2D data at Terrebonne

Bad channels with large spikes in the shot gathers were killed, although some shot gathers still contain interferences from nearby seismic exploration activities. Such interference is separable using f-k dip filtering when the reflection has reverse dip from the original data; interferences from reflections with the same dip is inseparable. Surgical mutes were also applied to some shot gathers to minimize data loss from these effects. Coherent noise, including tail buoy noise, bird noise, and mechanic streamer noise were also eliminated using f-k dip filtering. After filtering, shot gathers were transformed to CDP gathers with maximum fold between 3 and 9 depending on the shot interval along different profiles. Supergathers were generated from CDP gathers (9 each) for semblance velocity analysis and the resultant velocity analysis was smoothed to create a 2D velocity field for each profile. After this analysis, a prestack Kirchoff time migration was applied to the CDP gathers using the smoothed 2D velocity model.

The results from reprocessing of the 2D high-resolution multichannel seismic data allow for finer scale interpretations of the seismic images in the vicinity of the BSR. Nevertheless, these data still contain spikes, noise, and seismic interference from other nearby exploration activities.

683 Haines, et al. (2014) also discuss some inherent limitations in the processing and interpretation of
684 these data due to the geological complexity of the region. Such limitations may result from: i)
685 unrectified vertical offsets between intersecting profiles due to off-line received energy,
686 especially for deeper reflections, ii) side sweeping energy during acquisition due to the direction
687 of recording on migrated profiles, and iii) low CDP fold due to short streamer offsets and
688 variable CDP fold due to variable shot intervals along different profiles. Maximum fold
689 decreases substantially for shot intervals > 25 m. Combined, these acquistion and geometric
690 factors are critical in determining the resolution of 2D seismic data and the nature and character
691 of the BSR on seismic images.